IEICE TRANS. ELECTRON., VOL.E104–C, NO.10 OCTOBER 2021

INVITED PAPER *Special Section on Microwave and Millimeter-Wave Technologies*

Recent Progress on High Output Power, High Frequency and Wide Bandwidth GaN Power Amplifiers

Masaru SATO[†a)], ***Senior Member***, **Yoshitaka NIIDA**[†], **Atsushi YAMADA**[†,††], **Junji KOTANI**[†,††], **Shiro OZAKI**[†,††], **Toshihiro OHKI**[†], **Naoya OKAMOTO**[†,††], ***and*** **Norikazu NAKAMURA**[†,††], ***Nonmembers***

SUMMARY This paper presents recent progress on high frequency and wide bandwidth GaN high power amplifiers (PAs) that are usable for high-data-rate wireless communications and modern radar systems. The key devices and design techniques for PA are described in this paper. The results of the state-of-the art GaN PAs for microwave to millimeter-wave applications and design methodology for ultra-wideband GaN PAs are shown. In order to realize high output power density, InAlGaN/GaN HEMTs were employed. An output power density of 14.8 W/mm in S-band was achieved which is 1.5 times higher than that of the conventional AlGaN/GaN HEMTs. This technique was applied to the millimeter-wave GaN PAs, and a measured power density at 96 GHz was 3 W/mm. The modified Angelov model was employed for a millimeter-wave design. W-band GaN MMIC achieved the maximum P_{out} of 1.15 W under CW operation. The PA with Lange coupler achieved 2.6 W at 94 GHz. The authors also developed a wideband PA. A power combiner with an impedance transformation function based on the transmission line transformer (TLT) technique was adopted for the wideband PA design. The fabricated PA exhibited an average P_{out} of 233 W, an average PAE of 42 %, in the frequency range of 0.5 GHz to 2.1 GHz.

key words: *GaN power amplifier, InAlGaN/GaN HEMT, millimeter-wave, power amplifier, transmission line transformer, wide bandwidth*

1. Introduction

To date, interest in Gallium nitride (GaN) high power amplifiers (PAs) for applications such as wireless communications, space technology, electronic warfare systems, and test equipment has been increasing. The power amplifier, as a key element of RF transmitters, directly and significantly affects operational quality in these applications [1]–[3].

A current and prospective technology trend indicates three major directions in the use of RF PAs, which are high output power, high efficiency and high frequency and/or wide bandwidth. Higher output from PAs can extend range performance of communication equipment, radar and so on [4]–[6]. Higher efficiency of PAs [7], [8] make it possible to simplify cooling systems and reduce the size of the radio equipment. GaN is an attractive choice due to its high electron mobility, high electron saturation velocity, and high breakdown electrical-field [9]–[12]. This is the driving force for RF designers to introduce GaN high electron mobility transistors (HEMT) to radio transmitters.

Manuscript received December 31, 2020.
Manuscript revised February 13, 2021.
Manuscript publicized March 12, 2021.
[†]The authors are with Fujitsu Laboratories, Atsugi-shi, 243–0197 Japan.
[††]The authors are with Fujitsu, Atgugi-shi, 243–0197 Japan.
a) E-mail: sato.masaru@fujitsu.com
DOI: 10.1587/transele.2021MMI0001

Applications for broadband multifunctional RF system have made high frequency and wide-band PAs. In the case of wireless communication, the higher the frequency, the more bandwidth can be used to transmit high data-rate signals [13]. A wideband signal carries substantially more information than a narrow-band signal [14], [15]. For many of these systems, further increased bandwidth operation is strongly required for many of these systems [16], [17]. In the case of radar, range resolution of the radar depends on the bandwidth of the transmitted pulse [18]. In order to widen the bandwidth, several architectures for wideband amplifier designs have been reported, such as distributed amplifiers [19], [20] and reactive match amplifiers [21], [22]. In both types of amplifiers, wideband impedance transformation is the common point. Since the input and output impedances of a high-power amplifier decrease to a few ohms, wideband and low-loss impedance transformation from a few ohms to 50 Ω is necessary for realizing high power PAs.

To satisfy these requirements, we have developed innovative GaN device and RF design techniques. These techniques can be regarded as predecessors towards modern wireless communication and other radio transmission systems.

In Sect. 2, device fabrications for higher output power are described. Over the past decade, AlGaN/GaN HEMTs have been attracting a lot of attention as high power amplifiers owing to their high breakdown voltage characteristics [6], [10], [23], [24]. The authors reported an alternative approach employing an InAlGaN barrier layer [25] for microwave PA. InAlGaN HEMT technology was also adopted into a millimeter-wave amplifier [26], [27].

Conventional device models are insufficient to simulate output impedance properties, such as drain voltage dependence of S_{22} in short channel GaN HEMTs. The modified Angelov model of GaN transistors [28], [29] to design a millimeter-wave power amplifier is introduced in Sect. 3. The measured results of W-band PAs are shown in Sect. 4.

In Sect. 5, the design technique for ultra-wideband amplifiers is described. In order to combine multiple transistor units to increase output power from PAs, we introduced a novel four-way transmission line transformer (TLT) based planar power combiner with an impedance transformation function in order to expand the bandwidth of the GaN PA [30]. Section 6 concludes this work.

2. GaN HEMT Technology for Microwave to Millimeter-Wave Amplifiers

A schematic cross-sectional view of our InAlGaN/GaN HEMT is shown in Fig. 1. We introduced an indium-added InAlGaN barrier layer because the sheet resistance can be reduced without increasing tensile-strain, which cannot be avoided for an AlGaN barrier layer. Strain can be reduced even with a high Al composition. This allows the HEMT to simultaneously achieve high sheet carrier density and high electron mobility. All epitaxial layers were grown on a semi-insulating SiC substrate by metal-organic vapor phase epitaxy (MOVPE). On the lower side of the GaN channel layer, the InGaN back barrier was inserted to reduce the off-state drain leakage current. A regrown n+-GaN layer was used to reduce the ohmic contact resistance and ohmic electrodes consisting of Ti/Al were formed on the n+-GaN layer by an evaporation and lift-off technique [25].

A HEMT with 0.25 μm technology was fabricated. The maximum drain current and maximum transconductance were 1,058 mA/mm and 488 mS/mm, respectively. The measured cut-off frequency (f_t) and maximum oscillation frequency (f_{max}) were 20.7 GHz and 84 GHz, respectively.

The large signal measurement was carried out using the test structure with a total gate width of 1 mm. P_{in}-P_{out} characteristics were measured at the frequency of 3 GHz with a pulse width and a duty cycle of 10 μs and 10%, respectively. Figure 2 shows the drain bias dependence of the saturated output power density. As the drain voltage was increased, output power was also increased. The maximum output power density was 14.8 W/mm at a drain voltage of 90 V. The output power decreased when the drain bias was increased to 100 V. This decrease in the output power is caused by heat retention. This can be improved by conducting heat using a diamond heat spreader and was discussed in detail in [25]. An AlGaN/GaN HEMT test structure with the same gate width was also fabricated and measured for comparison. The measured power density was 9.6 W/mm at a drain voltage of 65 V. Thus, the power density of InAlGaN HEMT is 1.5 times higher than that of AlGaN HEMT technology.

InAlGaN/GaN HEMT technology was also applied to millimeter-wave PAs [26], [27]. HEMT with 80nm technology was used. Furthermore, a multi-layer passivation film was adapted. Electron traps in the passivation layer and semiconductor surface cause current collapse, which degrades output power and PAE. To decrease the electron traps, reducible silicon nitride was used to decrease oxidation on the surface of the semiconductor. Two anti-oxidational silicon nitride layers were used to decrease the electron traps in the film and on the surface [27].

The photograph of the test structure is shown in Fig. 3 (a). The gate width was 40 μm with 4 fingers. Figure 3 (b) shows the measured small signal gain of the millimeter-wave GaN HEMT. Drain and gate bias were 20 V and −1 V, respectively. The measured f_T and f_{max} were 90 GHz and 250 GHz, respectively.

Figure 4 (a) shows the large signal characteristics of the fabricated InAlGaN/GaN HEMT using a W-band load pull measurement system. The measured P_{in}-P_{out} characteristic

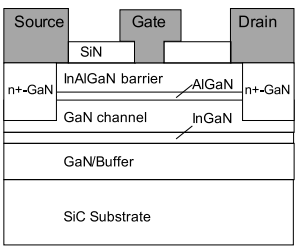

Fig. 1 Schematic cross-sectional view of InAlGaN/GaN HEMT on SiC substrate.

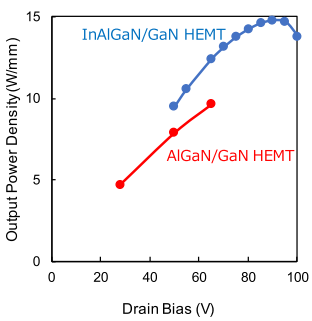

Fig. 2 Large signal characteristics of transistor comparing between InAlGaN/ and AlGaN/GaN HEMT.

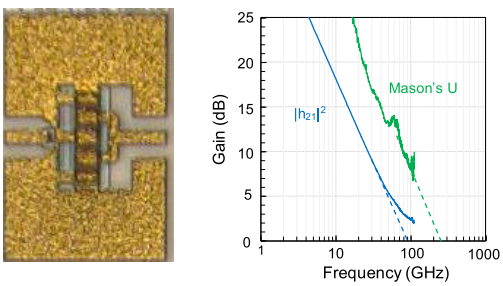

Fig. 3 (a) Photograph of Test Structure, (b) Small signal gain.

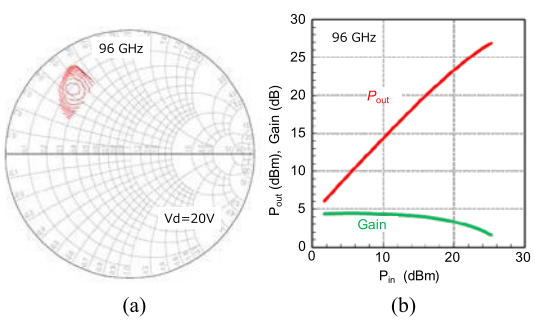

Fig. 4 (a) Loadpull measurement result of the fabricated InAlGaN/GaN HEMT, (b) P_{in}-P_{out} characteristic at 96 GHz.

at a frequency of 96 GHz is shown in Fig. 4 (b) [26]. The developed HEMT demonstrated an excellent power density of 3.0 W/mm at 96 GHz with the bias of 20V under continuous wave (CW) operation. High current density and low current collapse of the developed InAlGaN-barrier HEMT improved the power density significantly.

3. Millimeter-Wave GaN Device Modeling

We employed an Angelov GaN model, which is a well-used and well-known GaN HEMT model [31]. The conventional device models are insufficient to simulate the output impedance properties such as drain voltage dependence of S_{22} in a short channel GaN HEMT. This causes discrepancies between load-pull measurement and simulation at the millimeter-wave frequency range. Figure 5 shows the equivalent circuit of the Angelov GaN HEMT model [29], [31]. Model parameters were extracted from the measured DC I_D-V_D and S-parameters of the fabricated HEMT.

Figure 6 (a) shows the measured S_{22} at drain voltages of 5, 10, and 15 V. The measurements were done in the frequency range from 0.1 GHz to 26.5 GHz. These impedance traces of V_{DS} dependence cannot be expressed with conventional models.

We extracted the V_{DS} dependence of the output resistance R_{DS} and the capacitance C_{DS} in Fig. 7 from the measured S_{22} at 2 GHz [28] with the following simplified admittance equation:

$$\frac{1}{R_{DS}} + j\omega C_{DS} \cong \frac{1}{50} \times \frac{1 - S_{22}}{1 + S_{22}}. \quad (1)$$

Since the estimated R_{DS} and C_{DS} have V_{DS} dependence in the short channel GaN HEMT, we embed the V_{DS} dependence of the C_{DS} in the Angelov GaN model. The C_{DS} model equation is as follows:

$$C_{DS} = C_{DSP} + C_{DS0}(1 - tanh(\alpha \times V_{DS})). \quad (2)$$

Figure 6 (b) shows the simulated S_{22} from 0.1 GHz to 90 GHz with the Angelov GaN model. The crossover trajectory can be simulated when C_{DSP} is 20 fF, C_{DS0} is 60 fF, and α is 0.07.

The model parameters are extracted to fit the model simulation with the measured S-parameters, in particular the reflection parameters of S_{11} and S_{22} which are important to design the input and output matching circuits of power amplifiers. Furthermore, to check the usability of the extracted Angelov GaN model parameters in millimeter power amplifier design, a load-pull simulation was done at 90 GHz. The optimum load impedance was simulated to be 28 Ω + j 50 Ω and this agreed well with the load-pull measurement of 31 Ω + j50 Ω after a few extracted parameters were tuned. The load-pull characteristics at 90 GHz were compared with the measurement results and Angelov GaN model simulation at drain voltages of 10 V and 20 V in Fig. 8 (a), (b). The model simulation result and measurement results are in good agreement. Thus, these measurements confirm that the Angelov GaN model parameters can be used in the design of millimeter-wave power amplifiers.

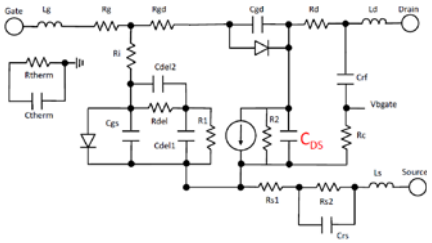

Fig. 5 Equivalent circuit of the Angelov GaN HEMT model [29], [31].

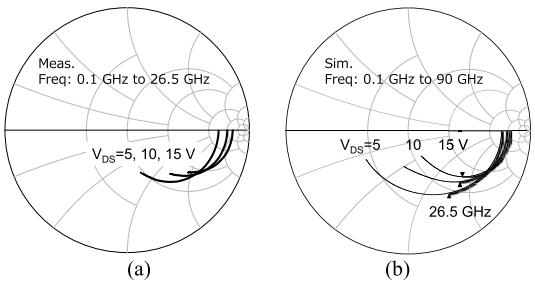

Fig. 6 (a) Measured S_{22} with V_{DS} from 0.1 to 26.5 GHz, (b) Simulated S_{22} with modified Angelov model from 0.1 to 90 GHz.

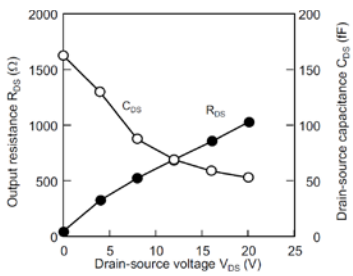

Fig. 7 V_{DS} dependence of R_{DS} and C_{DS} extracted from S_{22} at 2 GHz [28].

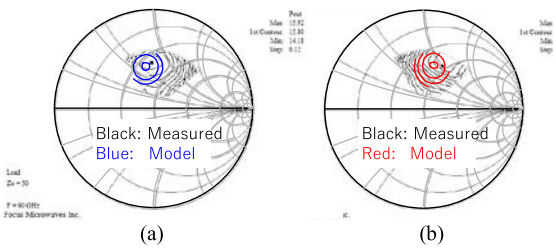

Fig. 8 Comparison of load-pull simulation and measured results of 90 GHz load-pull. (a) V_{DS} = 10 V, (b) V_{DS} = 20 V.

4. Millimeter-Wave GaN Power Amplifiers

A W-band MMIC was designed using coplanar waveguides because they can reduce the source inductance. First, a unit gate width of the PA stage to satisfy the power target was designed. As the unit gate width increases, the gain at millimeter-wave decreases due to gate resistance. A unit transistor with the unit gate width of 40 μm and four fingers was chosen. The InAlGN/GaN HEMT has a power

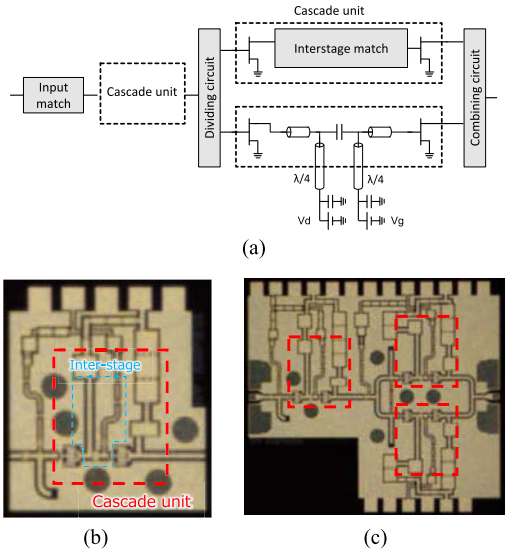

Fig. 9 (a) Schematic of W-band MMIC, (b) Chip photograph of the MMIC1, (c) Chip photograph of MMIC2.

density of 3 W/mm at a drain voltage of 20 V. This power density suggests that the two unit transistors whose unit gate periphery is 4×40 μm can deliver an output power of approximately 1W.

Second, an output combining circuit consisting of a series of lines and short stubs was used for the output-stage design. Then, an inter-stage matching circuit followed by the driver transistor was designed as shown in Fig. 9 (a). The inter-stage circuit consists of a series of lines, and two short stubs with capacitance, and the capacitance was large enough for the frequency range. Using these design procedures, a cascade unit was designed (MMIC1). Third, by combining the cascade units, W-band PA MMICs were designed (MMIC2) [32].

Figure 9 (b) shows the photograph of the cascade unit as MMIC1. It was used for the verification of the design. The gate width of the HPA was 160 μm. The chip size was 0.9×1.0 mm^2. Figure 9 (c) shows a photograph of the W-band PA as MMIC2, consisting of a cascade unit as the driving circuit, two cascade units connected in parallel, and a combining stage. The gate width of the HPA was 320 μm. The chip size was 2.0×1.8 mm^2.

RF performances were measured after assembling the MMICs on Cu plate. Figure 10 (a) shows the measured S-parameters of the fabricated MMICs at a drain voltage of 20 V. Dashed and solid lines represent the measured results of MMIC1 and MMIC2, respectively. Gain of the MMIC1 and MMIC2 at 86 GHz were 8.4 and 17.8 dB, respectively. The maximum gain of MMIC2 was 18.9 dB at 84 GHz and 3 dB bandwidth was from 77.8 to 89 GHz.

Large signal measurements of the MMIC2 were done at 86 GHz, CW mode and a drain voltage of 20 V, as shown in Fig. 10 (b). Solid and dashed lines show the measured and simulated results, respectively. Maximum output power was 1.15 W, the power density was 3.6 W/mm, and the

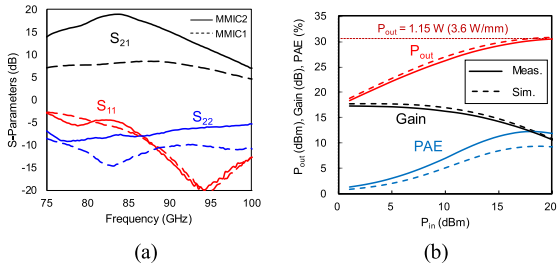

Fig. 10 (a) Measured S-parameters of the fabricated W-band MMICs. (b) Large-signal characteristics of MMIC2.

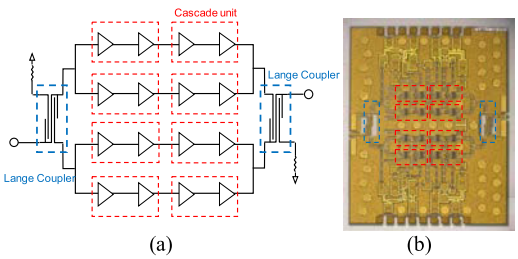

Fig. 11 W-band GaN PA with Lange coupler. (a) schematic of the MMIC3, (b) chip microphotograph of MMIC3.

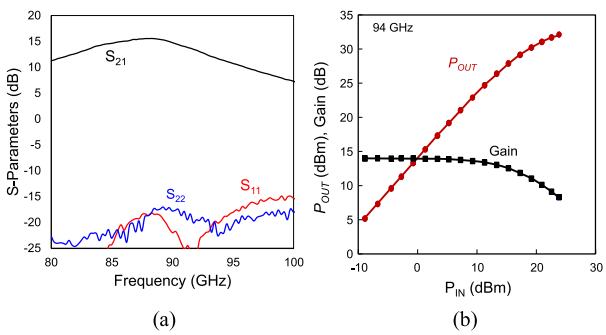

Fig. 12 (a) Measured S-Parameters of MMIC3. (b) Large signal measurement results.

maximum PAE was 12.3 %. The simulation results are in good agreement with the measured ones. Thus, the developed modified Angelov model works well for millimeter-wave MMIC design.

To increase the output power further, we employed a Lange coupler for W-band PA [33]. Figure 11 (a) shows a simplified schematic of the PA that consists of cascade units and Lange couplers at the input and output as MMIC3. Figure 11 (b) shows a chip microphotograph. The chip size was 2.3×2.9 mm^2. The Lange coupler had an insertion loss of less than 1 dB from the test structure measurements. The total gate width of HPA was 640 μm.

Figure 12 (a) shows the measured and simulated S-Parameters of the MMIC3 at a drain voltage of 20 V. The gain was 17 dB at a frequency of 88 GHz. Figure 12 (b) shows the P_{in}-P_{out} characteristic of MMIC3 measured at 94 GHz. The saturated power was 1.62 W, and the corresponding power density was 2.53 W/mm.

5. Broadband Amplifier Design

The key to realizing a broadband amplifier is to reduce the combining loss of the power combiner over a wide frequency range. Generally, the output impedance of the transistor is as low as a few ohms, because multiple transistors are laid out in parallel. Therefore, a wideband and low-loss impedance that transforms from a few ohms to 50 Ω is necessary. The transmission line transformer (TLT) is a type of wideband impedance transformer [34]. Rather than a conventional impedance transformer [35], which transfers energy by magnetic coupling, energy is transferred by a transverse transmission-line mode. This results in the realization of an ultra-wideband impedance transformer. By applying the TLT to a power combiner, wideband GaN PA can be utilized.

Figure 13 shows a circuit schematic of the proposed PA with a four-way power combiner with an impedance transformation function. Two stage power combiners (C1, C2) transform the impedance from 12.5 Ω to 50 Ω. An output matching circuit (OMC) transforms the impedance from 12.5 Ω to a few ohms. As the impedance ratio between the stages of the proposed circuit remain small, a wideband PA can be utilized.

In our work, the TLT was designed in a planar form, and broadside coupled lines were patterned on the top and bottom of the substrate to realize a strong coupling between the lines. The backside of the substate was hollowed out more than 10 mm from a metal block to reduce the insertion loss of TLT. The TLT can have its operating mode changed wideband balun, delay line, and phase inverter by changing the position of ground connection [36].

When the ground is connected at the center of the load as shown in Fig. 14 (a), the signal goes from the left to right,

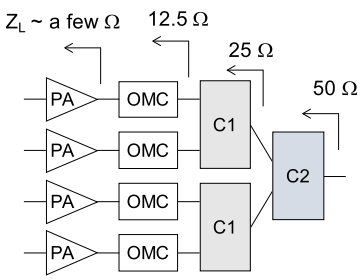

Fig. 13 Circuit schematic of the proposed PA with four-way power combiner with impedance transformation function.

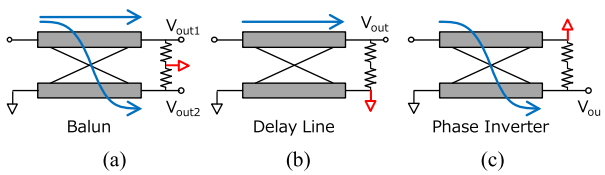

Fig. 14 Variation of TLT element by changing the ground connection. (a) Balun, (b) Delay line, (c) Phase inverter.

split into the top and bottom lines, with a phase difference of 180 degrees. It operates as a balun. When the ground is connected at the bottom of the load as shown in Fig. 14 (b), it operates as a delay line. When the ground is connected at the top of the load, the signal coming from the left is transmitted to the other side of the line, with a phase difference of 180 degrees. It operates as a phase inverter, as shown in Fig. 14 (c).

Figure 15 shows the schematic of the two-way combiner consisting of the TLT balun, delay line, and phase inverter. To design the four-way combiner, three two-input one-output power combiners were stacked as C1 and C2, illustrated in Fig. 13. As this power combiner is constructed by the TLT elements, the overall performance of this combiner can be wideband.

Figure 16 shows the fabricated broadband power amplifier consisting of 1:4 divider, input matching circuit (IMC), GaN HEMTs, OMC, and 4:1 combiner. The size of the jig was 22 × 27 cm and the jig under the TLT combiner had 15 mm hollowed out. A MEGTRON 6 substrate, with a dielectric constant and thickness of 3.4 and 0.5 mm respectively, was used. The impedance of the TLT was controlled by changing the width of the transmission lines. Metallized through-holes were formed in the substrate, and the bottom and top layer were electrically connected, to create a TLT-based power combiner. A GaN HEMT on SiC with 0.25 μm technology was used.

Figure 17 shows the measurement results of S-Parameters at a drain voltage of 50 V. A gain of over 9.7 dB and an input return loss of below −7.9 dB over the

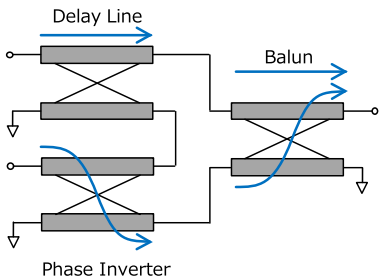

Fig. 15 Two-way power combiner using three TLT elements by changing the ground connection.

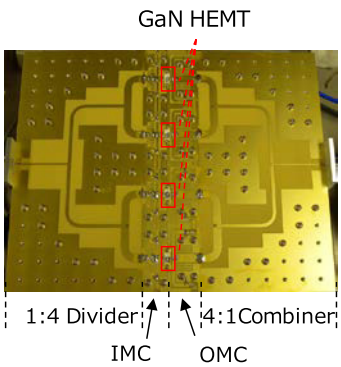

Fig. 16 Photograph of the fabricated wide bandwidth PA.

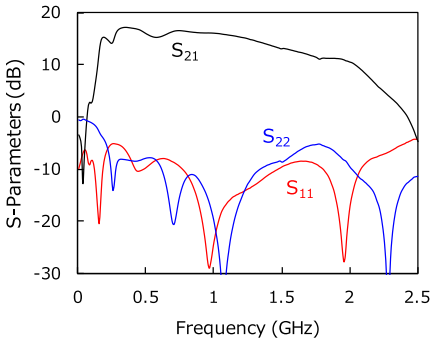

Fig. 17 S-Parameters of the wide bandwidth PA.

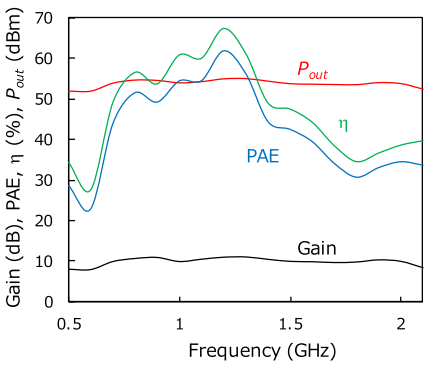

Fig. 18 Frequency dependence of the large signal characteristics of the wide bandwidth PA.

Table 1 Performance comparison of the wideband PAs.

Ref.	Freq. (GHz)	FBW (%)	Pout (W)	PAE (%)
[37]	1.55-2.25	36.8	100-110	60-70
[38]	1.1-2.0	58.1	200-223	40-52
[39]	0.9-1.8	66.7	96	52-59
[40]	2.0-2.7	29.8	100-158	55-65
[41]	0.1-1.8	179.9	93-141	35-68
[42]	0.1-3.0	187.1	107-148	25-48
[30] TLT-based PA	0.5-2.1	123	151-315	23-62

0.5–2.1 GHz range were achieved under a drain voltage of 50 V.

Large signal measurements under a condition of a 10 μs pulse width and a 1 percent duty cycle were evaluated under the drain voltage of 50 V. For an input power of 44 dBm, the PA produced an output of 53.4 dBm ± 1.6 dB at a PAE of 42.3 ± 19.4 % at the range of 0.5 GHz to 2.1 GHz as shown in Fig. 18. The peak P_{out} of 55 dBm (315 W) and the maximum PAE of 61.7 % were achieved at 1.3 GHz and 1.2 GHz, respectively.

Table 1 compares the published wideband PAs with a similar frequency range. The fractional bandwidth (FBW) is defined as

$$FBW = \frac{f_H - f_L}{f_C}, \tag{3}$$

where f_H, f_C, and f_L are the highest, center, and lowest frequency of the band, respectively. Comparing with reported wideband PAs in the same frequency range, the developed PA exhibited a wider bandwidth than the reported PAs with an output power over 200 W.

Furthermore, we recently reported differential mode TLT combiner which exhibited a large second-harmonic suppression [43].

6. Conclusion

This paper presented GaN HEMT PAs to realize advanced wireless communication and radar systems. To realize a high output power density, InAlGaN/GaN HEMTs were introduced. The power density was 14.8 W/mm in the S-band, which is 1.5 times higher than that of an AlGaN/GaN HEMT. This technology was also applied to millimeter-wave PAs. The power density was 3 W/mm at 96 GHz. W-band InAlGaN/GaN MMIC achieved P_{out} of 2.6 W at 94 GHz. We also developed a novel design technique for wideband power amplifiers. A power combiner with an impedance transformation function based on the TLT was employed. The fabricated PA exhibited an output power of 233 W, PAE of 42 %, in the frequency range of 0.5 to 2.1 GHz.

Acknowledgments

The authors would like to thank the device development team at Fujitsu Lab. for the GaN fabricating process. The authors would like to Dr. K. Makiyama and Dr. K. Joshin for their contribution to these works. Part of this work has been achieved by the “Agile Deployment Capability of Highly Resilient Optical and Radio Seamless Communication System,” with the commissioned research of National Institute of Information and Communications Technology (NICT). Part of this work was partially supported by Innovative Science and Technology Initiative for Security, ATLA, Japan.

References

[1] D. Kuchta, D. Gryglewski, and W. Wojtasiak, “A GaN HEMT Amplifier Design for Phased Array Radars and 5G New Radios,” Micromachines 2020, vol.11, no.4, 2020.
[2] A. Nelander and Z. Tóth-Pál, “Modular System Design for a New S-Band Marine Radar,” 2009 International Radar Conference “Surveillance for a Safer World”, 2009.
[3] Y. Itoh and K. Honjo, “Fundamental Perspective of Future High Power Devices and Amplifiers for Wireless Communication Systems,” IEICE Trans. Electron., vol.E86-C, no.2, pp.108–119, Feb. 2003.
[4] J. Gallagher, J.A. Haimerl, T. Higgins, and M. Gruber, “Space Fence Radar Leverages Power of GaN,” Microwave Journal, pp.4–9, Sept. 2018.
[5] M.J. Pelk, W.C.E. Neo, J.R. Gajadharsing, R.S. Pengelly, and L.C.N. de Vreede, “A High-Efficiency 100-W GaN Three-Way Doherty Amplifier for Base-Station Applications,” IEEE Trans. Microw. Theory Techn., vol.56, no.7, pp.1582–1591, July 2008.
[6] Y. Kobayashi, S. Yoshida, Z. Yamamoto, and S. Kawasaki, “S-Band GaN on Si Based 1kW-Class SSPA System for Space Wireless Applications,” IEICE Trans. Electron., vol.E96-C, no.10, pp.1245–1253, Oct. 2013.
[7] P. Hindle, “Going Green: High Efficiency GaN Amplifier,” Microwave Journal, pp.23–28, Sept. 2018.

[8] T. Sugiura, S. Furuta, T. Murakami, K. Tanji, N. Otani, and T. Yoshimatsu, "High Efficiency Class-E and Compact Doherty Power Amplifiers with Novel Harmonics Termination for Handset Applications," IEICE Trans. Electron., vol.E102-C, no.10, pp.699–706, Oct. 2019.
[9] A. Wakejima, K. Matsunaga, Y. Okamoto, Y. Ando, T. Nakayama, K. Kasahara, and H. Miyamoto, "280 W Output Power Singe-ended Amplifier using Single-die GaN-FET for W-CDMA Cellular Base Stations," Electronics Letters, vol.41, no.18, pp.1004–1005, 2005.
[10] T. Kikkawa, T. Maniwa, H. Hayashi, M. Kanamura, S. Yokokawa, M. Nishi, N. Adachi, M. Yokoyama, Y. Tateno, and K. Joshin, "An over 200-W Output Power GaN HEMT Push-pull Amplifier with High Reliability," Proc. IEEE MTT-S International Microwave Symposium, pp.1347–1350, 2004.
[11] T. Palacios, A. Chakraborty, S. Rajan, C. Poblenz, S. Keller, S.P. DenBaars, J.S. Speck, and U.K. Mishra, "High-Power AlGaN/GaN HEMTs for Ka-Band Applications," IEEE Electron Device Lett., vol.26, no.11, pp.781–783, Nov. 2005.
[12] K. Joshin and T. Kikkawa, "High-Power and High-Efficiency GaN HEMT Amplifiers," Proc. IEEE Radio and Wireless Symposium, pp.65–68, 2008.
[13] S. Shinjo, M. Hangai, Y. Yamaguchi, and M. Miyazaki, "Advanced GaN HEMT Modeling Techniques and Power Amplifiers for Millimeter-Wave Applications," Proc. IEEE MTT-S International Microwave Symposium, pp.566–569, 2020.
[14] C.M. Cooke, K.M.K.H. Leong, A. Escorcia, K. Nguyen, X.B. Mei, J. Arroyo, T.W. Barton, D.L. Wu, and W.R. Deal, "A 220-GHz InP HEMT Direct Detection Polarimeter," IEEE Trans. Microw. Theory Techn., vol.67, no.12, pp.5191–5201, Dec. 2019.
[15] H. Hamada, T. Fujimura, I. Abdo, K. Okada, H. Song, H. Sugiyama, H. Matsuzaki, and H. Nosaka, "300-GHz, 100-Gb/s InP-HEMT Wireless Transceiver Using a 300-GHz Fundamental Mixer," Proc. IEEE MTT-S International Microwave Symposium, pp.1480–1483, 2018.
[16] A. Ghavidel, F. Tamjid, A. Fathy, and A. Kheirdoost, "GaN Widening Possibilities for PAs," IEEE Microw. Mag., pp.46–55, 2017.
[17] M. Roberg, S. Schafer, O. Marrufo, and T. Hon, "A 2–20 GHz Distributed GaN Power Amplifier Using a Novel Biasing Technique," Proc. IEEE MTT-S International Microwave Symposium, pp.694–697, 2019.
[18] J. Oh, J. Jang, C.-Y. Kim, and S. Hong, "A W-Band 4-GHz Bandwidth Phase-Modulated Pulse Compression Radar Transmitter in 65-nm CMOS," IEEE Trans. Microw. Theory Techn., vol.63, no.8, pp.2609–2618, 2015.
[19] S. Masuda, "Advances in GaN HEMT MMIC Amplifiers," 2010 Asia-Pacific Microwave Conference, WS2A-4, 2010.
[20] C.F. Campbell, S. Nayak, M. Kao, and S. Chen, "Design and Performance of 16-40 GHz GaN Distributed Power Amplifier MMICs Utilizing an Advanced 0.15 μm GaN Process," Proc. IEEE MTT-S International Microwave Symposium, 2016.
[21] Y. Niida, Y. Kamada, T. Ohki, S. Ozaki, K. Makiyama, N. Okamoto, M. Sato, S. Masuda, and K. Watanabe, "X-Ku wide bandwidth GaN HEMT MMIC Amplifier with Small Deviation of Output Power and PAE," Proc. IEEE Compound Semiconductor Integrated Circuit Symposium, 2014.
[22] E. Kuwata, K. Yamanaka, H. Koyama, Y. Kamo, T. Kirikoshi, M. Nakayama, and Y. Hirano, "C-K Band Ultra Broadband GaN MMIC Amplifier with 20 W Output Power," Proc. Asia-Pacific Microwave Conference, pp.1558–1561, 2011.
[23] S. Nuttinck, E. Gebara, B. Banerjee, S. Venkataraman, J. Laskar, and H.M. Harris, "Applications of GaN Microwave Electronic Devices," IEICE Trans. Electron., vol.E86-C, no.8, pp.1409–1415, Aug. 2003.
[24] A. Corrion, C. Poblenz, P. Waltereit, T. Palacios, S. Rajan, U.K. Mishra, and J.S. Speck, "Review of Recent Developments in Growth of AlGaN/GaN High-Electron Mobility Transistors on 4H-SiC by Plasma-Assisted Molecular Beam Epitaxy," IEICE Trans. Electron., vol.E89-C, no.7, pp.906–912, July 2006.
[25] T. Ohki, A. Yamada, Y. Minoura, K. Makiyama, J. Kotani, S. Ozaki, M. Sato, N. Okamoto, K. Joshin, and N. Nakamura, "An Over 20-W/mm S-Band InAlGaN/GaN HEMT with SiC/Diamond-Bonded Heat Spreader," IEEE Electron Device Lett., vol.40, no.2, pp.287–290, Feb. 2019.
[26] K. Makiyama, S. Ozaki, T. Ohki, N. Okamoto, Y. Minoura, Y. Niida, Y. Kamada, K. Joshin, K. Watanabe, and Y. Miyamoto, "Collapse-Free High Power InAlGaN/GaN-HEMT with 3 W/mm at 96 GHz," Proc. IEEE International Electron Devices Meeting, 2015.
[27] K. Makiyama, Y. Niida, S. Ozaki, T. Ohki, N. Okamoto, Y. Minoura, M. Sato, Y. Kamada, K. Joshin, K. Watanabe, and Y. Miyamoto, "High-Power-Density InAlGaN/GaN-HEMT Technology for W-band Amplifier," Proc. IEEE Compound Semiconductor Integrated Circuit Symposium, 2016.
[28] K. Joshin, S. Ozaki, T. Ohki, N. Okamoto, Y. Niida, and K. Makiyama, "Millimeter-wave GaN HEMT Model with V_{ds} Dependence of C_{ds} for Power Amplifier Applications," Proc. Asia-Pacific Microwave Conference, pp.582–584, 2014.
[29] K. Joshin, K. Makiyama, S. Ozaki, T. Ohki, N. Okamoto, Y. Niida, M. Sato, S. Masuda, and K. Watanabe, "Millimeter-Wave GaN HEMT for Power Amplifier Applications," IEICE Trans. Electron., vol.E97-C, no.10, pp.923–929, Oct. 2014.
[30] Y. Niida, M. Sato, M. Nishimori, T. Ohki, and N. Nakamura, "An over 230 W, 0.5-2.1 GHz Wideband GaN Power Amplifier using Transmission-Line-Transformer-Based Combining Technique," Proc. IEEE MTT-S International Microwave Symposium, pp.25–28, 2020.
[31] Verilog-A definition of Angelov GaN FET in Agilent Advanced Design System (ADS) 2012.08.
[32] Y. Niida, Y. Kamada, T. Ohki, S. Ozaki, K. Makiyama, Y. Minoura, N. Okamoto, M. Sato, K. Joshin, and K. Watanabe, "3.6 W/mm High Power Density W-band InAlGaN/GaN HEMT MMIC Power Amplifier," Proc. IEEE Topical Conference on Power Amplifiers for Wireless and Radio Applications, pp.24–26, 2016.
[33] M. Sato, "GaN HEMT Technology for W-Band High Power Amplifiers," European Microwave Conference, Workshop WS-02-6, 2017.
[34] J. Sevick, Transmission Line Transformers, 4th ed., 2001.
[35] J. Cho, K. Lim, S. You, M. Seo, K. Kim, J. Sim, M. Park, and Y. Yang, "Design of a 100 Watt High-Efficiency Power Amplifier for the 10-500 MHz Band," Proc. Asia Pacific Microwave Conference, pp.285–288, 2009.
[36] G. Boeck, "Modeling and Design of Multilayer Transmission Line Transformers and Baluns," Proc. IEEE International Conference on Microwave and Optoelectronics, pp.230–232, 2005.
[37] A.A. Tanany, D. Gruner, and G. Boeck, "Harmonically Tuned 100 W Broadband GaN HEMT Power Amplifier with more than 60% PAE," Proc. European Microwave Conference, pp.159–162, 2011.
[38] M.T. Arnous, K. Bathich, S. Preis, and G. Boeck, "Harmonically-Tuned Octave Bandwidth 200 W GaN Power Amplifier," Proc. European Microwave Integrated Circuit Conference, pp.429–432, 2012.
[39] S. Preis, D. Gruner, and G. Boeck, "Investigation of Class-B/J Continuous Modes in Broadband GaN Power Amplifiers," Proc. IEEE MTT-S International Microwave Symposium, 2012.
[40] P. Saad, D. Maassen, and G. Boeck, "Efficient and Wideband Two-Stage 100 W GaN-HEMT Power Amplifier," Proc. European Microwave Integrated Circuit Conference, pp.337–340, 2014.
[41] K. Krishnamurthy, D. Lieu, R. Vetury, and J. Martin, "A 0.1–1.8 GHz, 100 W GaN HEMT Power Amplifier Module," Proc. IEEE Compound Semiconductor Integrated Circuit Symposium, 2010.
[42] B.A. Ezzeddine, A. Hung, E. Viveiros, and H. Huang, "Ultra Wide-Band, High-Power, High-Efficiency GaN Amplifier," Proc. IEEE International Wireless Symposium (IWS), 2013.
[43] Y. Niida, M. Sato, T. Ohki, and N. Nakamura, "A 0.6–2.1-GHz Wideband GaN High-Power Amplifier Using Transmission-Line-Transformer Based Differential-Mode Combiner with Second-Harmonic Suppression," IEEE Trans. Microw. Theory Techn., vol.69, no.3, pp.1675–1683, March 2021.

Masaru Sato received the B.E. and M.E. degrees in electrical engineering from Tohoku University, in 1996 and 1999, respectively. He received the Ph.D. degree in electronics and applied physics from Tokyo Institute of Technology in 2014. He joined Fujitsu Laboratories Ltd., Atsugi, Japan, in 1999, where he has been engaged in research on high-speed InP-based HEMT circuits for fiber-optic communication systems and millimeter-wave integrated circuits. From 2009 to 2010, he was with Georgia Institute of Technology, where he researched high-frequency analog CMOS circuits. His current research interests include the development of microwave and millimeter wave MMICs. He was a recipient of the Young Researcher's Award from the IEICE in 2006.

Yoshitaka Niida received the B.S., M.S., and Ph.D. degrees in physics from Tohoku University in 2005, 2009, and 2012, respectively. In 2012, he joined Fujitsu Laboratories Ltd., where he is currently engaged in research and development work on GaN HEMT high power amplifiers.

Atsushi Yamada received the B.E., M.E. and Ph.D. degrees in electronic engineering from Tohoku University, Sendai, Japan, in 2000, 2002 and 2005, respectively. In 2005, he joined in Fujitsu Laboratories Ltd., Atsugi, Japan, and he was involved in the development of SiGe HEMTs for RF devices. Since 2006, he has been engaged in crystal growth of GaN by MOVPE. His current research interests include the development of next-generation GaN HEMT technologies.

Junji Kotani received the B.E. and M.E., and Ph.D. degrees in electrical engineering from Hokkaido University, Sapporo, Japan, in 2003, 2005 and 2008, respectively. He joined Eindhoven University of Technology, Eindhoven, Netherlands, in 2008, where he has been engaged in research on long-wavelength InAs quantum dot lasers. In 2010, he joined Fujitsu Laboratories Ltd., Atsugi, where he is currently engaged in research and development of GaN HEMT high power amplifiers. From 2017, he has served as a principal investigator for the next-generation high power amplifiers, which has been supported by ATLA, Japan.

Shiro Ozaki received the B.E. and M.E. degrees from Yokohama National University, in 2002 and 2004, respectively. He received the Ph.D. degree from Hokkaido University in 2019. In 2004, he joined Fujitsu Laboratories Ltd., Atsugi, and has been engaged in advanced materials for semiconductor devices. His current research interests include process technology for GaN HEMTs. He was a recipient of the He Bong Kim Award (Honorable Mention) from the International Conference on Compound Semiconductor Manufacturing Technology (CS-MANTECH), in 2016.

Toshihiro Ohki received the B.E. and M.E. degrees in electrical engineering from Waseda University, Tokyo, Japan, in 1999 and 2001, respectively. Since 2001, he has been with Fujitsu Laboratories Ltd., Atsugi, Japan, where he was engaged in the research and development of InP-based RTD/HEMTs and GaN-based HEMTs for high speed optical and wireless communication systems. He is a member of the Japan Society of Applied Physics.

Naoya Okamoto received the B.E., M.E., and Ph.D. degrees from Osaka University, Osaka, Japan, in 1988, 1990, and 2001, respectively. In 1990, he joined Fujitsu Laboratories Ltd. and has gained a range of experience in areas such as crystal growth, process, device evaluation and circuit design of compound semiconductor electron devices. He has also worked as a researcher at the Nanoelectronics Collaborative Research Center of The University of Tokyo from 2002 to 2004. He is currently engaged in the research and development of GaN, InP-based high electron mobility transistors (HEMTs) and III-V nanowire devices. He is a member of IEEE.

Norikazu Nakamura received the B.E., M.E., and Ph.D. degrees in Engineering from Yokohama National University, Japan in 1993, 1995, and 1998, respectively. He joined Fujitsu Laboratories Ltd., Atsugi, Japan in 1998, where he had been engaged in research and development of diamond-related materials for magnetic media from 1998 to 2009. His current research interests include GaN-based high-power/high-frequency devices and microwave systems. From 2015 to 2018, he served as a principal investigator for the next-generation high power GaN HEMTs, which was supported by ATLA, Japan. He is currently a head of devices & materials research center.